JETIR.ORG

ISSN: 2349-5162 | ESTD Year : 2014 | Monthly Issue



JOURNAL OF EMERGING TECHNOLOGIES AND INNOVATIVE RESEARCH (JETIR)

An International Scholarly Open Access, Peer-reviewed, Refereed Journal

SIMULATION BASED TEMPERATURE DEPENDENT PERFORMANCE STUDY OF SOLID OXIDE FUEL CELL

¹Vishnu Tej Gunisati, ¹Vasu Vijay Singh, ¹Saumya Kumar, ²Samita Maitra

¹Students, Department of Chemical Engineering, B.M.S. College of Engineering, Bengaluru, India ²Professor, Department of Chemical Engineering, B.M.S. College of Engineering, Bengaluru, India

Abstract: Conventional energy sources such as petroleum and coal are currently the primary sources for electricity production. However, these energy sources are depleting, and are also unfriendly to the environment. Renewable energy sources such as solar energy, wind energy, photovoltaic cell energy etc. are very effective in reducing the greenhouse gas emissions serving as cleaner alternatives. Solid oxide fuel cells (SOFC) serve as one such alternate clean source of energy. These unlike other fuel cells which can only operate with specific fuel sources, exhibit fuel flexibility by operating at high temperatures. These high temperature operations however come with several inherent challenges such as suitable choice of material, stability of the auxiliary systems and so on, for the optimum performance of the fuel cell. Hence critical understanding of corelation between high temperatures and the performance of the SOFC is required so that the controlling factors can be optimised further to suit more small-scale applications. To aid this aspect in our study, simulation of a three-dimensional modelled single cell planar solid oxide fuel cell was performed under steady-state and counter-current flow condition in the temperature range of 500°C to 1200°C using a computational dynamics software, COMSOL Multiphysics. The choice of materials for the fuel cell involved the use of, nickel oxide as anode, lanthanum strontium cobalt ferrite as cathode and yttria-stabilized zirconia the electrolyte. Hydrogen was supplied as anode side fuel while oxygen was fed as the cathode side fuel. The performance of the fuel cell was then determined from the polarization and power characteristics, which were then analyzed, and it was finally interpreted that with the increase in operating temperature, the performance of the solid oxide fuel cell increases.

Index Terms - SOFC, COMSOL, Temperature, Polarization, Power.

I. INTRODUCTION

Energy demands currently are being met via fossil fuel-based sources such as petroleum and coal, but these are diminishing on a relatively rapid scale with unfavourable environmental impacts. Alternative energy sources such as renewable energy systems (RE) are becoming more common in power generation applications. RE sources include solar energy, wind energy, photovoltaic (PV) cell energy, fuel cell etc. which are very effective in reducing the greenhouse gas emissions. Soon, major portions of rise in electrical energy demand will be met by widespread installation of distributed power generation [1]. Amidst these renewable energy sources is the fuel cell, which is an electrochemical cell that converts chemical energy obtained from fuel into electrical energy and produces fewer pollutants (water and heat). Therefore, fuel cells are considered as a low pollution power sources among other power conversion technologies [2]. Generally, fuel cells have significant advantages, such as they can be placed anywhere in the system, high power quality, reliability, and improved efficiency. Fuel cells can be used in transportation, stationary power generation and battery replacement [3]. In general, solid oxide fuel cells (SOFC) have high electrical efficiency and relatively low cost compared to other types of fuel cells such as alkaline fuel cell (AFC), proton exchange membrane (PEM) fuel cell. Both natural gas and coalderived gas are used as the primary sources of fuel for SOFCs. Since SOFCs operate at higher temperatures, it is possible to use other fuels such as Methane (CH₄) and produce Hydrogen (H₂) internally, with the help of a metal catalyst. Hence, the practical difficulty of externally feeding pure H₂ can be eliminated. In this respect, we use the term fuel flexibility. Some of the other advantages of SOFCs are simpler concept, design and construction, higher efficiency, fuel flexibility and relatively high-power density [4], [5]. But these high temperature operations present several inherent challenges for operation in terms of suitable choice of material, stability of the auxiliary systems and so on, therefore critically understanding of the effect of temperature on performance of the SOFC becomes important, so that the controlling factors can be optimised further to suit more small-scale applications.

To evaluate the performance of the SOFC several simulation-based works have been carried out previously such as R. Yadav, et al. [6] have used MATLAB/SIMULINK environment to create a 2D flow diagram for their modelling and simulation. Gebregergis A, et al. [7] proposed a method to analyze the dynamic response of a SOFC by distributed modelling approach and lumped modelling. The distributed model and lumped model was implemented by PSpice software to obtain theoretical results such as polarization curves. R. Bianchi, et al. [8] evaluated the SOFC performance through electrochemical impedance spectra (EIS) analysis and characteristic curves and proposed 2D steady state simulation code. This model was implemented in Fortran. S. N. Ranasinghe et. al [9] had carried out the temperature dependent study for different gas flow patterns but for only three different operating temperatures, using COMSOL indicating the correlation between temperature and performance of the SOFC and characterizing it. Hence in our survey it was seen that a combined work on temperature dependent behavior of SOFC followed by the critical analysis of the nature of the performance curves is yet to be carried out for wider operating temperature conditions to get a more complete understanding of the performance of the solid oxide fuel cell.

To aid this aspect in our study a stationary 3D modelled planar solid oxide fuel cell was prepared and analysed via finite element analysis, under steady state conditions for specific counter current gas flow pattern over a wide operating temperature range between 500°C to 1200°C. First the correct operation of the created fuel cell model was verified via the simulation images, then the characterisation of the performance of the fuel cell was done through the polarization characteristics and power characteristics using COMSOL Multiphysics (version 5.1) and then finally the nature of the curves obtained were analysed to identify the controlling factors.

II. METHODOLOGY

2.1 Details of the analytical tool

COMSOL Multiphysics is a cross-platform finite element analysis, solver, and Multiphysics simulation software. It allows conventional physics-based user interfaces and coupled systems of partial differential equations (PDEs). COMSOL provides an IDE and unified workflow for electrical, mechanical, fluid, acoustics, and chemical applications [10].

The experimental setup for this study is the SOFC (solid oxide fuel cell) model created using COMSOL Multiphysics (version 5.1) simulation software. Figure 1 shows the working interface of COMSOL Multiphysics [10].

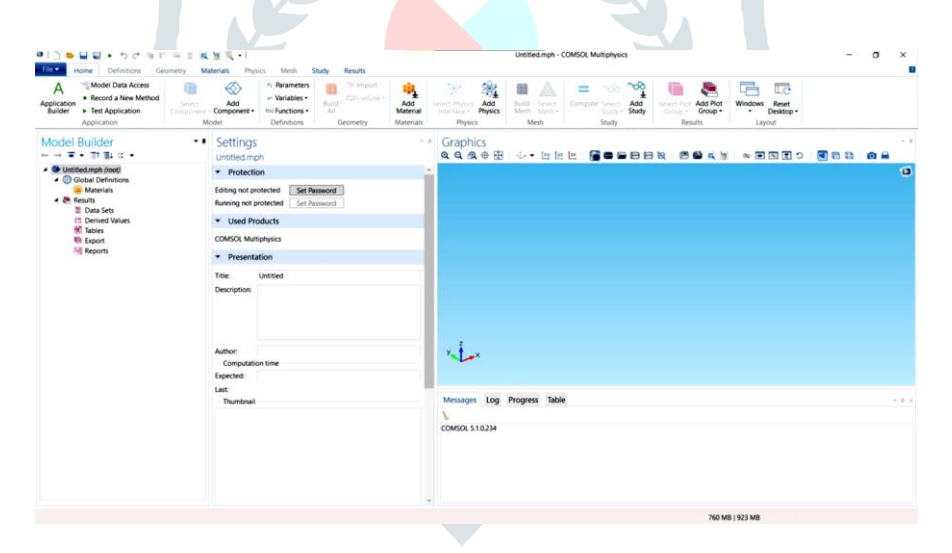


Figure 1: Interface of COMSOL Multiphysics

2.2 Components of the solid oxide fuel cell

SOFC has three main components the anode, cathode, and the electrolyte The choice of the materials for the study were done using the COMSOL Multiphysics software in the material selection sub section in the global definition section.

Firstly, nickel oxide (NiO) was selected as the anode material as it allows the oxygen ions that diffuse through the electrolyte to oxidize the hydrogen fuel serving as a catalyst and is the commonly used material [11]. Secondly the electrolyte considered for the study was yttria-stabilized zirconia (YSZ) due to superior stability at high temperature, good conductivity of oxygen ions and cost effectiveness [11], [12]. Lastly lanthanum strontium cobalt ferrite (LSCF) was selected as the cathode material because of good structural stability and high electrochemical activity for oxygen reduction reactions [13]. The cross-sectional view of SOFC is shown in figure 2.

Figure 2: Cross Sectional view of the SOFC

2.3 Overview of the operation of the solid oxide fuel cell

The conversion of fuel to electrical energy predominantly involves four steps in a fuel cell namely reactant transport (1), electrochemical reaction (2), ionic conduction (3) and product removal (4). These steps are schematically shown in figure 3 [14].

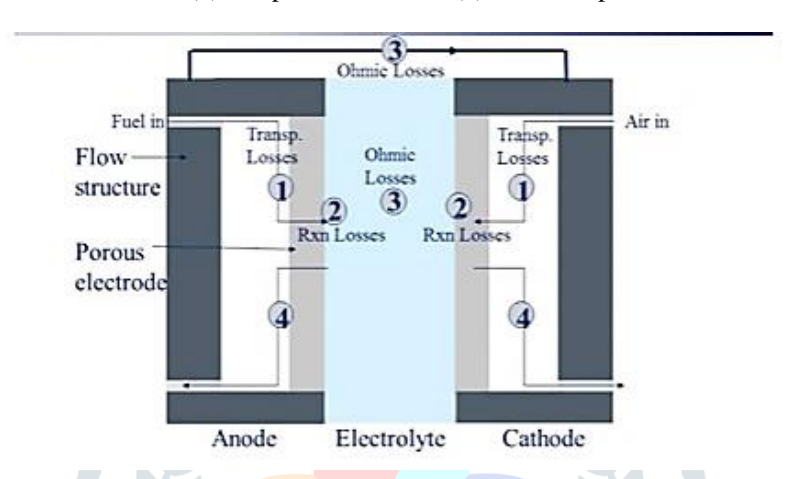


Figure 3: Cross-section of fuel cell illustrating major steps in electrochemical generation of electricity Source: Adapted from [14]

Firstly, efficient delivery of the reactants is brought about by the combined effect of the flow field plates and the porous electrode which distribute the fuel over the entire surface of the fuel cell. Then the fed reactants must undergo the electrochemical reaction to generate current. This is followed by ionic and electronic conduction where the ions produced or consumed during the electrochemical reaction must diffuse through the electrolyte (due to relatively larger nature of ions) and electrons produced or consumed must flow externally through the wire to maintain the charge balance. This is finally followed by efficient product removal, as buildup of unremoved by products such as water can eventually strangle the fuel cell preventing new fuel and oxidant from being able to react [14].

In our SOFC the hydrogen fuel is fed at the anode, and oxygen is supplied at the cathode. The high temperature enables internal fuel reforming and high ionic conductivity, helping in the reduction of oxygen molecules into ions which then diffuse through the electrolyte. The electrolyte selectively allows for only the oxygen ions to diffuse through it as diffusion of anions requires a much higher activation energy. The oxygen ions reach the anode where they combine with hydrogen to produce free electrons and water as the byproduct [12]. The free electrons generated pass through the external circuit across the load thereby providing electricity and also sustain the reaction at the cathode [11]-[14]. Figure 4 schematically indicates the overview of the operation of SOFC.

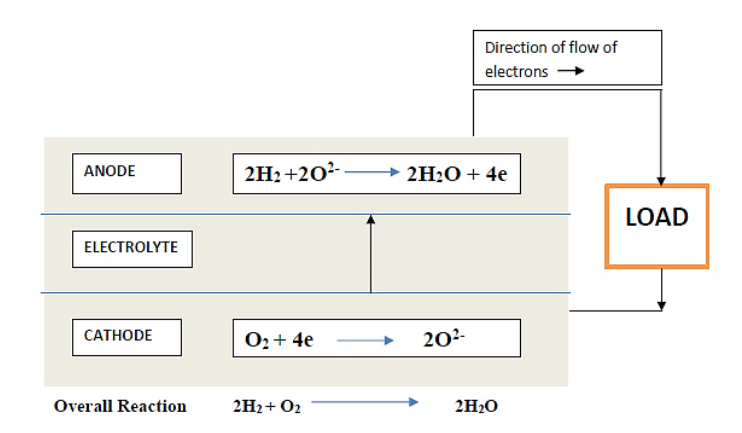


Figure 4: Electrochemical Reaction in the SOFC

2.4 Governing Equations Used for Modelling

The fundamental momentum, charge balance and mass transport equations were used in modelling the SOFC. The main processes associated with the functionality of the model are described as follows.

Firstly, for multicomponent transport, the mass balances for gas phase in gas channels and porous electrodes were modelled using Maxwell-Stefan Diffusion and Convective flow equations. When considering the transport of fluid, both diffusion (the distribution of chemical species uniformly in space with time) and convection (the bulk motion of fluid) of the fluid were included for each electrode flow compartment (anode and cathode flow channels). The material transport was modelled by the Maxwell-Stefan's diffusion and convection equations over Fick's diffusion [9], [15], [16]. The governing equation is given by equation 1,

$$\frac{\partial \rho \omega_i}{\partial t} + \nabla \cdot (j_i + \rho \omega_i u) = R_i \tag{1}$$

where, ω_i the mass fraction, ji is the molecular mass flux (mol/m²s), Ri is the reaction rate of the ith species and u is the velocity field.

Secondly, for the Gas Diffusion aspect, flow distribution in gas channels was modelled using Navier-Stokes equation. To define the velocity field and the pressure field in gas channels, we used a free and porous media flow interface. Gas flow in open channels was modelled by using the weakly compressible Navier-Stokes equation given by equation 2 [9], [17].

$$\rho\left(\frac{\partial u}{\partial t} + u \cdot \nabla u\right) = -\nabla p + \nabla(\mu(\nabla u) + (\nabla u)^T) - \frac{2}{3}\mu(\nabla u)I + F$$
 (2)

This equation is constructed by combining several independent parameters which are $\rho\left(\frac{\partial u}{\partial t} + u.\nabla u\right)$: Inertial forces of the system, ∇p : Force created by pressure of the fluid, $\nabla (\mu(\nabla u) + (\nabla u)^T) - \frac{2}{3}\mu(\nabla u)I$: Viscous forces of the system, and F: The external forces applied to the fluid.

Flow in the porous GDEs was then modelled using Brinkman equations. Here the flow velocities in the porous GDE'S were enforced with the help of the Brinkman equations given which were used to define the boundary conditions of the inlet channels (H₂ and O₂) while the outlet pressure is made equal to 1 atm. This is given by equation 3 [9], [18], [19],

$$\nabla p = -\left(\frac{\mu}{k}\right) * v + \mu_{\rm e} \nabla^2(v) \tag{3}$$

Where, μ_e is the parameter of efficient viscosity.

Finally, the charge balances (ionic and electronic) were modelled using Butler-Volmer charge transfer kinetics. A secondary current distribution interface was used to determine the ionic and electronic charge balances of the electrolyte. This includes the two GDEs as well as the anode and the cathode current feeders. We had assumed that the charge transfer current density can be described by using the Butler-Volmer charge transfer kinetics as it is the most fundamental equation that describes the relationship between the current through the electrolyte and the voltage difference between the electrodes and the bulk electrolyte [9], [20]. Anode charge transfer kinetics $(i_{a,ct})$ is given by the equation 4 as,

$$i_{a,ct} = i_{0,a}((\frac{ch2}{ch2\ ref})exp(\frac{0.5F}{RT}\eta) - (\frac{c_{h2o}}{c_{h2o,ref}})exp(\frac{-1.5F}{RT}\eta))$$
 (4)

where i_{0,a} is the anode exchange current density, (A/m²), c_{h2} is the molar concentration of H₂, (mol/m³), c_{h2o} is the molar concentration of H₂O,(mol/m³), c_t is the total concentration of species ,(mol/m³), c_{h2,ref} and c_{h2o,ref} is the reference molar concentrations,(mol/m³), F is the Faraday's constant, (coulomb/volt) and η is the overvoltage, (V).

Now cathode charge transfer kinetics are given by equation 5 as,

$$i_{c,ct} = i_{0,c} \left(exp\left(\frac{3.5F}{RT}\eta\right) - x_{02}\left(\frac{c_t}{c_{02,ref}}\right) exp\left(\frac{-0.5F}{RT}\eta\right) \right)$$
 (5)

where $i_{0,c}$ is the cathode exchange current density, (A/m^2) , x_{02} is the molar fraction of O_2 . For both the aforementioned equations the overvoltage is defined by equation 6 as [9], [20],

$$\eta = \varphi_{\text{electronic}} - \varphi_{\text{ionic}} - \Delta \varphi_{\text{eq}} \tag{6}$$

where $\Delta \phi_{eq}$ is the equilibrium potential difference.

We used the anode inlet voltage as a fixed reference voltage which is equal to zero, following which the cathode inlet voltage (Vcell) is given by equation 7 as [9], [21],

$$V_{\text{cell}} = \Delta \emptyset_{\text{eq,c}} - \Delta \emptyset_{\text{eq,a}} \tag{7}$$

For this model, we used $\Delta Ø_{eq,c} = 1~V$, $\Delta Ø_{eq,a} = 0~V~$ and $0.05V < V_{pol} < 0.8~V$.

2.5 Steps involved in simulation

The following step-by-step approach was followed in our research for modelling the SOFC.

First step involved selecting the physics and the study for the model. The cross section of the single cell SOFC shown in figure 2 was modelled using COMSOL Multiphysics software. Nickel oxide (NiO) was used as the anode material, while lanthanum strontium cobalt ferrite (LSCF) was used as the cathode material and the electrolyte was made of Yttria-Stabilized Zirconia (YSZ). In our model the anode fuel used was a mixture of H_2 and water vapour (humidified H_2O). In addition, a mixture of air, water vapour and nitrogen were used as the cathode fuel. Furthermore, the anode and the cathode were used as two porous gas diffusion electrodes (GDEs). To model the gas diffusion in the cell, we had used an anode flow channel along with a cathode flow channel [9].

Next, step involved constructing the 2D model. In this the geographical model was constructed first [9]. For our model, we had selected the y-z plane as the 2D plane. The established 2D model is shown in figure 5.

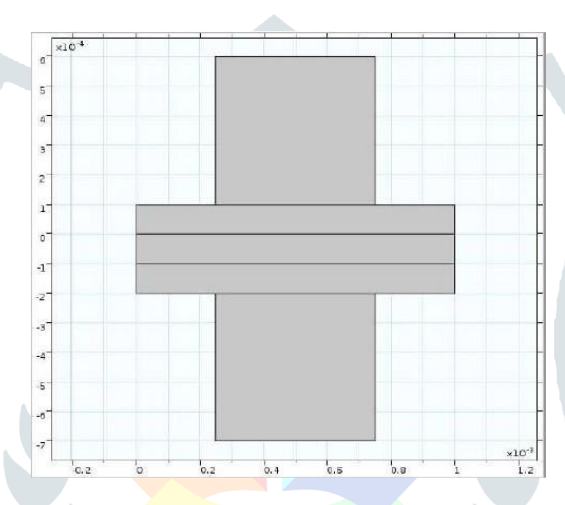


Figure 5: 2D model of SOFC in COMSOL

Next step involved extruding the 2D model to 3D. To create the 3D model, we extruded it [9]. In figure 6, the constructed 3D geographical model including two GDEs, electrolytes and the two gas flow channels, is shown.

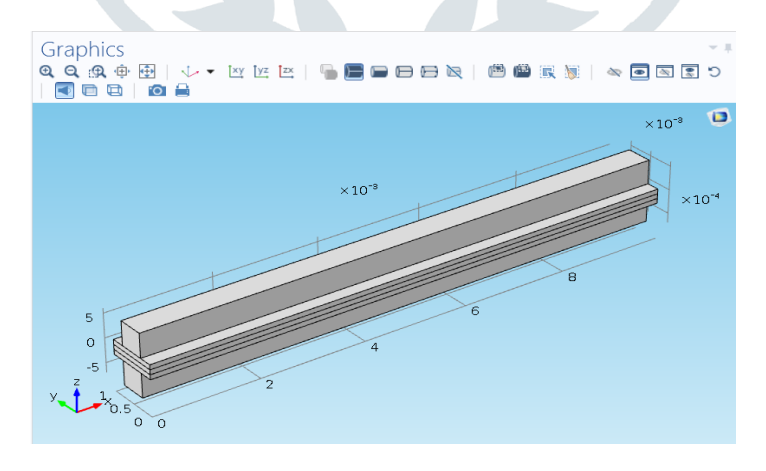


Figure 6: 3D model of the SOFC in COMSOL

The next step involved setting parameters according to requirements and assigning them for GDE's. The following parameters, like [9] were set for the analysis of the SOFC at different temperatures by the user as shown in table 1.

Table 1: List of the user defined parameters

Parameters	Associated values [units]
Atmospheric pressure	1 ATM
Temperature	800 °C
Viscosity, air	3E-5[Pa*s]
Pressure drop, anode	2[Pa]
Pressure drop, cathode	6[Pa]
Exchange current density, anode	$0.1[A/m^2]$
Exchange current density, cathode	$0.01[A/m^2]$
Specific surface area, anode	1E9[1/m]
Specific surface area, cathode	1E9[1/m]
Initial cell polarization	0.05[V]
Anode permeability	$1E-10[m^2]$
Cathode permeability	1E-10[m ²]
Equilibrium voltage, anode	0[V]
Equilibrium voltage, cathode	1[V]
Electrolyte effective conductivity, anode	1[S/m]
Electrolyte effective conductivity, cathode	1[S/m]
Solid effective conductivity, anode	1000[S/m]
Solid effective conductivity, cathode	1000[S/m]
Electrolyte conductivity	5[S/m]
Current collector conductivity	5000[S/m]
Porosity	0.4
Molar mass, H ₂	2[g/mol]
Molar mass, O ₂	32[g/mol]
Molar mass, H ₂ O	18[g/mol]
Gas flow channel width	0.5e-3[m]
Gas diffusion electrode thickness	1e-4[m]
Electrolyte thickness	1e-4[m]
Gas flow channel height flow channel length	0.5e-3[m]
Flow channel length	10e-3[m]

Next, we assigned the boundaries for the model. Here no slip conditions were assigned at the free and porous media flow interface for gas flow in open channels and slip conditions were assigned in the anode and the cathode [9].

The next step involved creating the mesh for the model [9]. After configuring the parameters, we had created the mesh to discretize the model as shown in figure 7. The finite element method which divides the model into small geometrical shapes was used so that we could get more accurate results for our simulations.

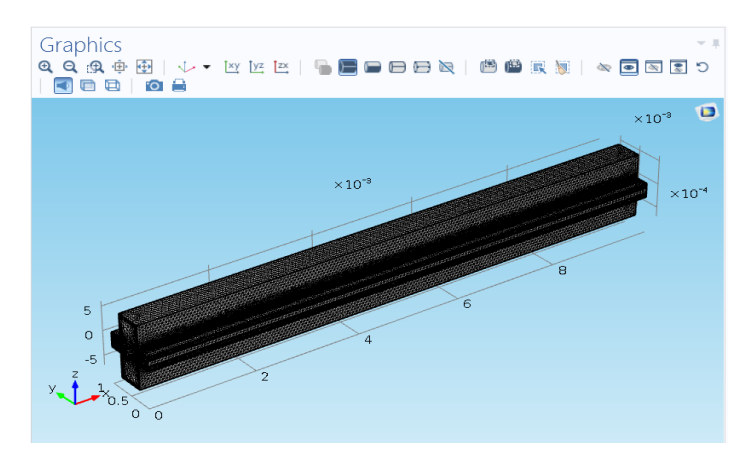


Figure 7- Meshed 3D model of SOFC created in COMSOL

Then we assigned other study parameters for the required outputs. For the analysis, we selected the stationary study mode assuming that the load and temperature are independent of the time. Simulation models were developed to evaluate the performance for counter flow gas flow pattern, we considered gas entering to the anode flow channel from the right side and the gas outlet on the left. Furthermore, for cathode flow channel, gas inlet on the left side while gas outlet on the right side. To evaluate the variation of characteristics with temperature, temperature values of the model are varied accordingly while keeping all the parameters constant. Finally, we ran the simulation and obtained the results [9].

III. RESULTS AND DISCUSSIONS

3.1 Simulated flow of ions in the fuel cell

The simulated flow of hydrogen and oxygen ions is shown here in figure 8 to further perceive and verify the correct operation of the modelled fuel cell. Here the dark red colour index indicates a high concentration of the ions, and the dark blue colour index indicates absence of ions, and the shades in between indicate decreasing concentration in order from darker shades of red followed by lighter shades of red to lighter shades of blue followed by darker shades of blue. The left end of the image represents the anode, and while the right end indicates the cathode.

The first image of figure 8 represents the flow of hydrogen ions. It can be here that the hydrogen ions remain localised at the anode and do not diffuse through the electrolyte. The second image in figure 8 shows that the oxygen ions diffuse through the electrolyte to reach the anode and carry out the electrochemical reaction as expected.

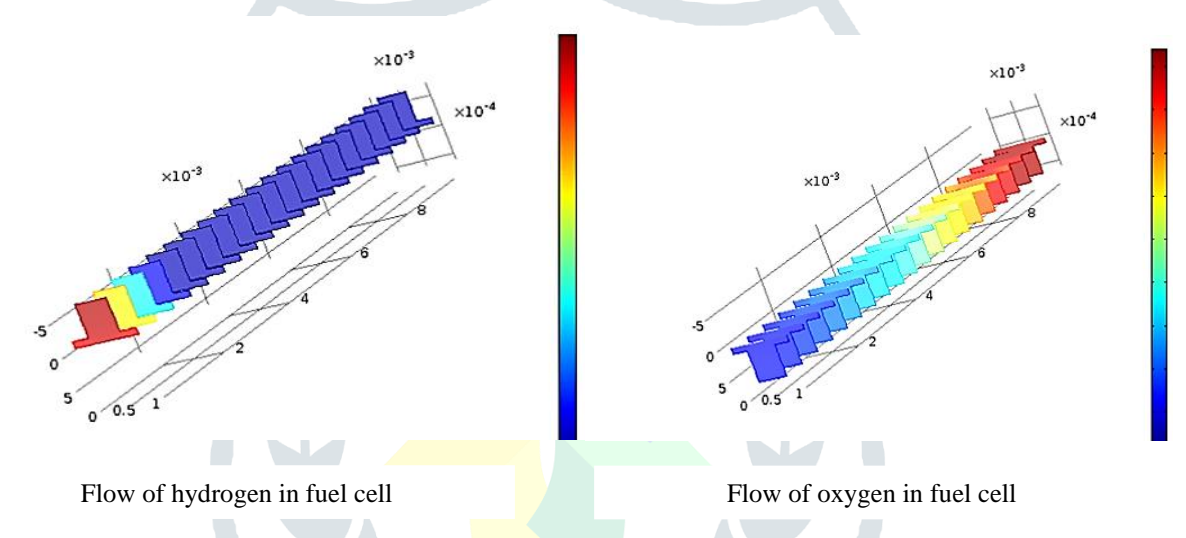


Figure 8: Simulation of flow of ions in the electrolyte in COMSOL

To evaluate the performance of the SOFC, the polarization characteristics and power characteristics curves were plotted and analysed.

3.2 Polarisation characteristics

The polarisation characteristics of a fuel cell depend on polarisation voltage and current density; hence we first define these terms. Current density is measure of current per unit active area of the electrode [22]. There are two different types of current densities, namely exchange current density and the average current density. Exchange current density is a measure of how easily the charges can overcome energy barrier to diffuse from the electrolyte to the catalyst surface and vice versa. It's the measure of electrode's readiness to proceed with an electrochemical reaction. While the average current density is the difference between anode and cathode exchange densities. The polarisation voltage indicates the voltage output of the fuel cell for a given average current density output [23], [24]. Therefore, polarisation characteristics of the fuel cell are determined by plotting the polarization voltage against average current density output for different operating temperatures. To further understand how these characteristics differ in reality and theory we first discuss the ideal polarisation curve and then shift our focus gradually to the actual polarisation curve obtained from our simulation study.

An ideal fuel cell would supply any amount of current (if it is supplied with sufficient fuel), while maintaining a constant voltage as determined by thermodynamics. In practice, however, the actual voltage output of a real fuel cell is less than the ideal thermodynamically predicted voltage. This arises due to three controlling factors as shown in the figure 9, firstly, the activation loses arising due to electrochemical reaction (shown by the region 1) affect the nature of the initial section of the curve, secondly, ohmic loses arising due to ionic and electronic conduction (shown by region 2) affect the nature of the mid-section of the curve, and finally, the concentration polarisation which arise due to mass transport (shown by the region 3) affect the nature of the final section of the curve [14], [24]-[26].

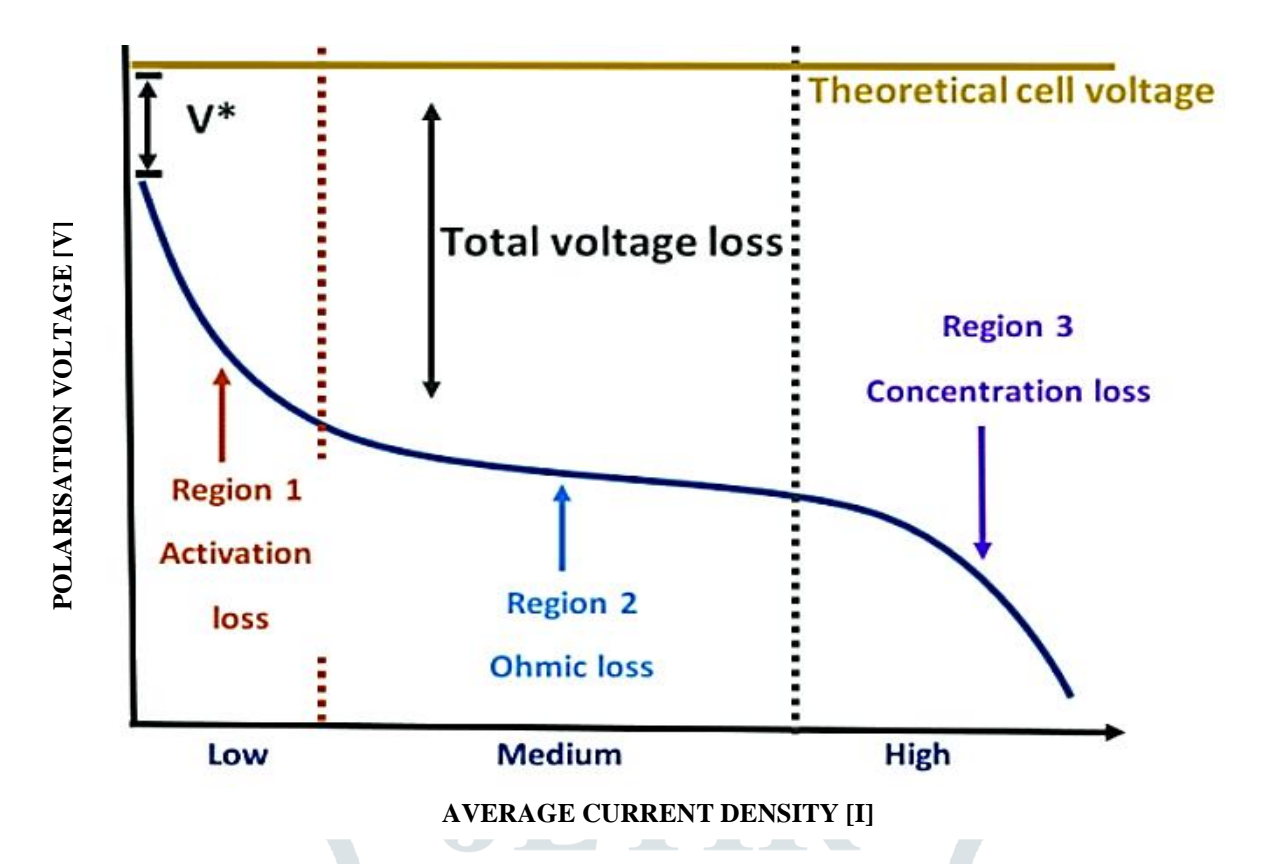


Figure 9: Schematic of fuel cell polarisation curve Source: Adapted from [27]

Therefore, in contrast to the constant value of the ideal, thermodynamically predicted polarisation voltage of a fuel cell (indicated by the golden line), the actual polarisation voltage of a fuel cell (indicated by the blue curve) is lower due to the mentioned irreversible losses and varies with average current density. It is given by equation 8 [14],

$$V = E_{thermo} - \eta_{act} - \eta_{ohmic} - \eta_{conc}$$
 (8)

Where, V is actual polarisation voltage (real output voltage of fuel cell), E_{thermo} is the theoretical polarisation voltage (thermodynamically predicted fuel cell voltage output); set by the laws of thermodynamics, η_{act} are the activation losses due to reaction kinetics, η_{ohmic} are the ohmic losses from ionic and electronic conduction, and η_{conc} are the concentration losses due to mass transport.

The polarisation characteristics of our SOFC were hence determined by plotting polarization voltage against average current density output for five different operating temperatures set as parameters which were 500, 800, 900, 1000 and 1200 degree centigrade. Data for one such curve at 800°C for average current density output and polarisation voltage is shown in table 2. Through the simulations performed under steady state condition and counter flow pattern of ions it can be interpreted from figure 10 that with increase in operating temperature, the SOFC maintains a high fuel cell polarisation voltage for a fixed current density output. It can also be seen that, at high operating temperatures the SOFC continues to provide polarisation voltage by maintaining high current density output without undergoing saturation at a lower value unlike at lower operating temperatures. Maintaining a high fuel cell voltage with high current density output is a desirable factor for indicating the performance of the SOFC, hence fuel cell voltage axis can be regarded as the efficiency axis [14]. Therefore, it can be inferred from figure 10 that the increase in operating temperature increases the performance of the fuel cell.

It is further observed that the jump in polarisation characteristics was almost insignificant on increasing the operating temperature from 800°C-900°C, but from 900°C-1000°C it was slightly more pronounced and then it was very significant from 1000°C-1200°C at higher current densities. This jump is also observed to be significant only in the later stages of the curve. This can be due to increase in temperature not having much effect on the activation loses but substantially reducing the ohmic loses and concentration polarisation, thereby influencing the nature of the curve. In addition, the reduction in the voltage loses is more prominent when the operating temperature is raised by the same factor of 200°C above 1000°C i.e., from 1000°C-1200°C than when raised below 1000°C i.e., from 800°C-1000°C.

Table 2: Polarization data at 800°C

Average Current density [I]	Polarisation voltage [V]
367.76223	0.95
668.370518	0.9
1085.633265	0.8
1421.350053	0.7
1756.80046	0.6
2077.571206	0.5
2353.746729	0.4
2561.772431	0.3
2709.994263	0.2

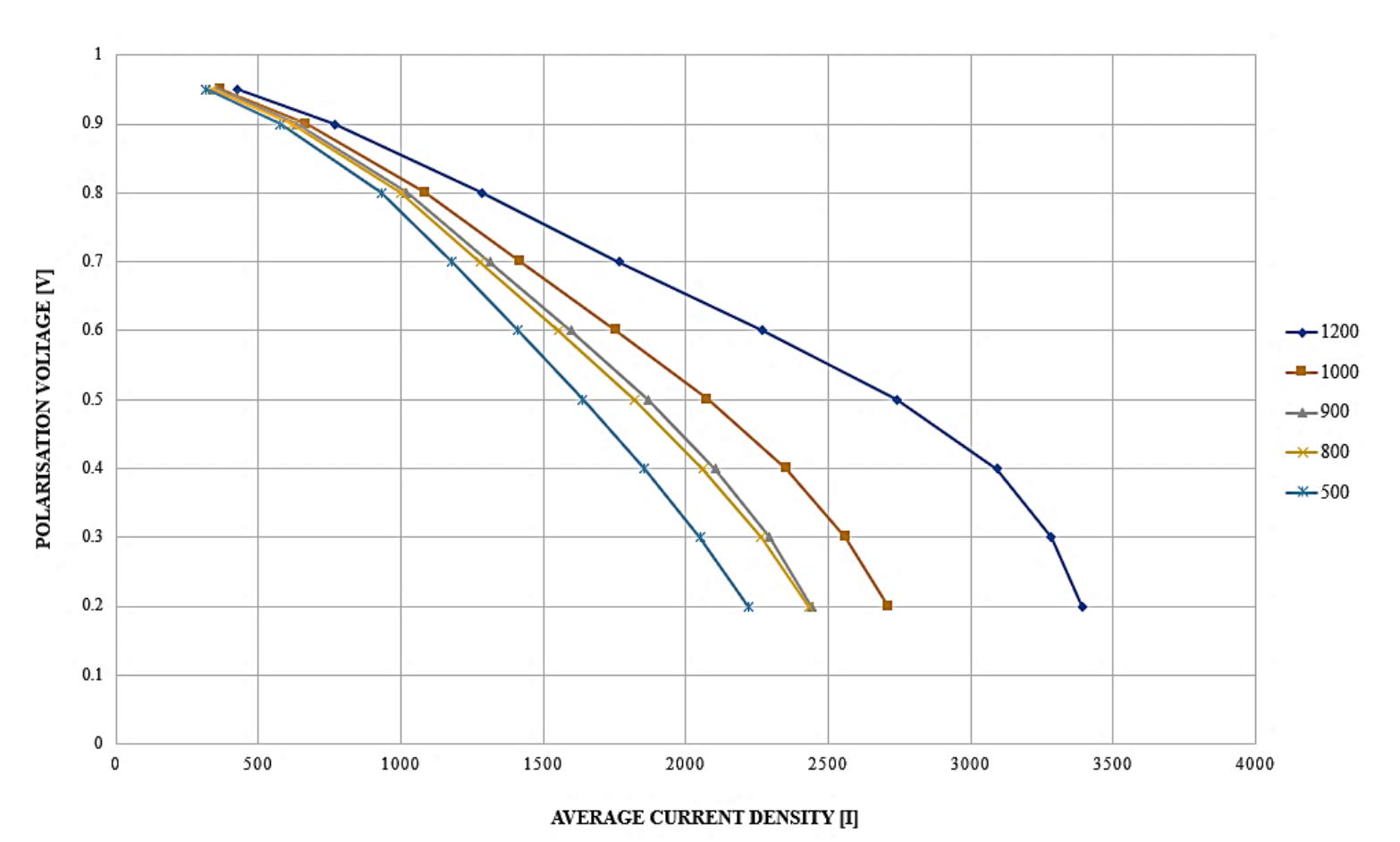


Figure 10: Polarization characteristics

3.3 Power characteristics

The power characteristics of SOFC involves the plot of power density output against average current density output for different operating temperatures of the fuel cell [28], hence we first define the term power density. Power density indicates how much power a fuel cell can produce per unit volume or per unit mass. The power delivered by the fuel cell (P) is the product of average current density output (I) and polarisation cell voltage output (V), which is given by equation 9 [14],

$$P = IV (9)$$

The power characteristics of our SOFC were hence determined by plotting the average cell power density output against average current density output for five different operating temperatures as parameters which were 500, 800, 900, 1000 and 1200 degree centigrade. Table 3 shows the average current density output and average cell power output data for one such curve at 800°C. From figure 11 it can be deducted from the simulations performed under steady state condition and counter flow pattern of ions that at high operating temperatures a higher average cell power is obtained for a fixed average current density output. In addition it is seen that the SOFC operates at high temperatures to provide the same power output in addition to maintaining high current density output without reaching saturation unlike at lower operating temperatures. As the ability of the SOFC to provide power output by maintaining a high current density output at the same time without saturation is a desirable characteristic [14], it can hence be inferred from figure 11 that the performance of the SOFC increases with increase in operating temperature.

In addition, due to dependence of cell power output on cell voltage, the nature of power characteristics curve is influenced by the same activation loses, ohmic loses and concentration polarisation effects. Further due to this dependence, when the operating temperature is shifted across from 500°C-1200°C, nature of the jump in the curve lies between being significant in the temperature range of 1000°C-1200°C and not so significant in the temperature range of 800°C-1000°C and involves a higher reduction in voltage loses beyond 1000°C as seen in figure 11.

The power density curve can also be constructed from the polarisation curve by multiplying the voltage at each point on the curve by the corresponding current density. Fuel cell power density increases with increasing current density, reaches a maximum, and then falls at still higher current densities. At current densities below the power density maximum, voltage efficiency improves but power density falls. While at current densities above the power density maximum, both voltage efficiency and power density fall. Hence the fuel cells are designed to operate at or below the power density maximum [14].

Average Current density [I]	Average cell power density [P]
Tiverage Current density [1]	Tiverage cen power density [1]
367.76223	349.3741185
668.370518	601.5334662
1085.633265	868.5066118
1421.350053	994.945037
1756.80046	1054.080276
2077.571206	1038.785603
2353.746729	941.4986915
2561.772431	768.5317294
2709.994263	541.9988526

Table 3: Power characteristics data at 800°C

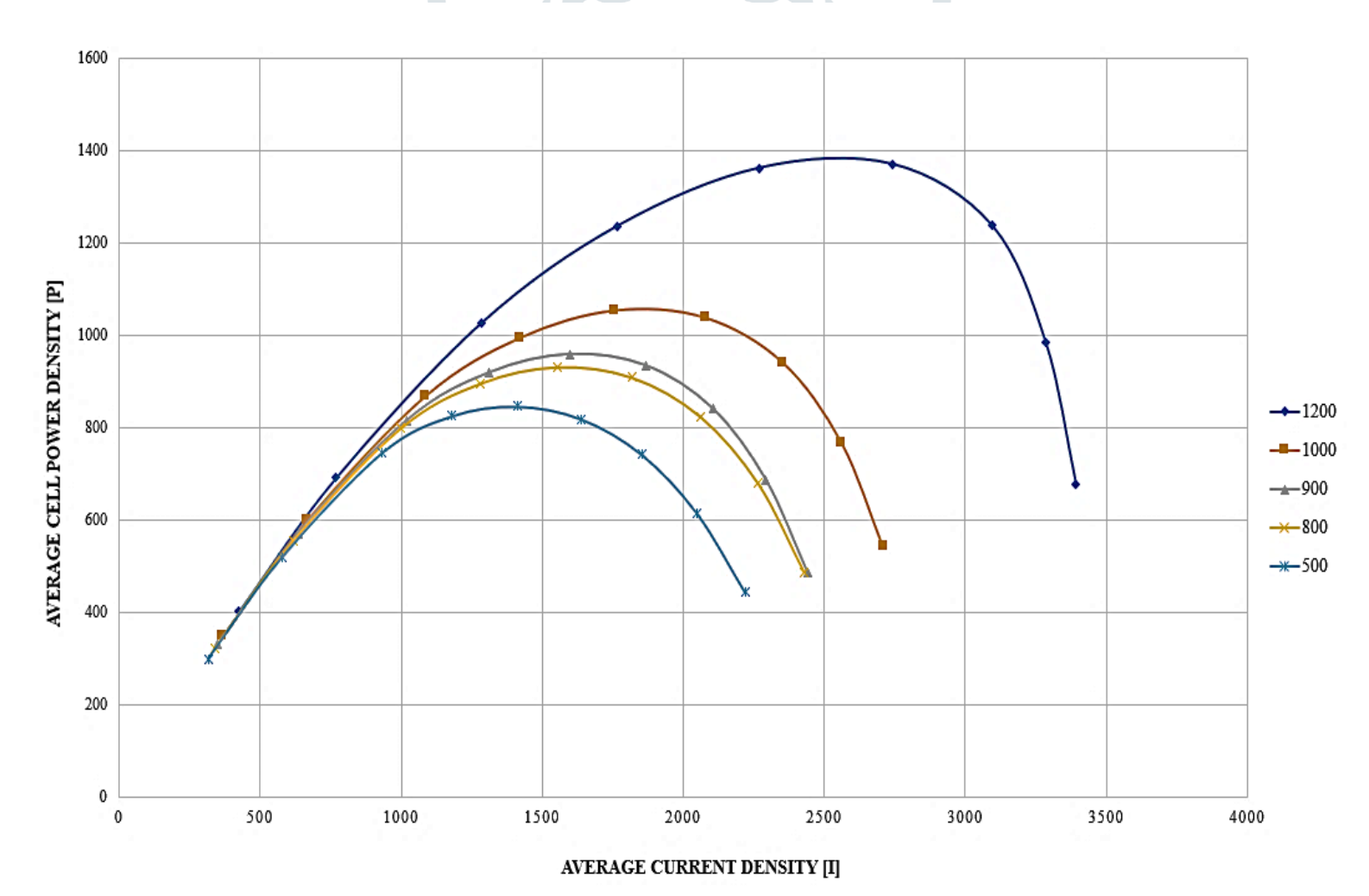


Figure 11: Power characteristics

IV. CONCLUSION

In this study, a steady state model for a single cell SOFC was developed using COMSOL Multiphysics software (version 5.1) to evaluate its performance under counter current gas flow pattern for five different operating temperatures (500°C, 800°C, 900°C, 1000°C and 1200°C). Firstly, we showed the image of simulation of flow of ions in our SOFC model which verified the correct operation of the modelled fuel cell. Then as per the computational results it was seen that, with the increase in operating temperature, the performance of the SOFC increases. It was also seen that the characteristic nature of the polarization and power characteristics curve was influenced by the activation loses, ohmic loses and the concentration polarization. In addition, a sudden jump was observed in both the curves, with the nature of the jump being significant between 1000°C-1200°C and not so significant between 800°C-1000°C, and higher reduction in voltage loses was seen beyond 1000°C when the operating temperature was shifted across from 500°C-1200°C. Hence finally in our study we were able to corelate the performance and temperature of the SOFC and analyze the performance curves.

To further extend the scope of this simulation, a study for different flow patterns could be carried out with a time dependent analysis, thereby further determining a dynamic model for SOFC operation. In addition, the reason for the sudden jump and the selective difference in reduction in voltage loses within a particular operating temperature range could be investigated further. Finally, upon combination of above studies modifications could be suggested to further enhance the performance of the solid oxide fuel cells.

REFERENCES

- [1] Fang Z. Peng, "Special issue on distributed power generation," IEEE Trans. Power Electron., vol. 19, no. 5, Sep. 2004
- [2] X. Li, Principles of Fuel Cell. Taylor and Francis, 2006, ISBN:1-59169-022-6.
- [3] S. Fedakar, S. Bahceci, and T. Yalcinoz, "Modeling and simulation of sofe using psead," in Eurocon 2013, July 2013, pp. 1058– 1065.
- [4] S. C. Singhal, "Solid oxide fuel cells," Winter 2007, Accessed: 29.09.2020. [Online]. Available: https://www.electrochem.org/dl/interface/wtr/wtr07/wtr07 p41-44.pdf
- [5] S. Chen, N. Lior, and W. Xiang, "Coal gasification integration with solid oxide fuel cell and chemical looping combustion for high-efficiency power generation with inherent {CO2} capture," Applied Energy, vol. 146, pp. 298 – 312, 2015.
- [6] Ruchi Yadav & Gauri Shankar, (2014). Modelling and Simulation of Solid Oxide Fuel Cell.
- [7] Gebregergis, A., P. Pillay, D. Bhattacharyya, and R. Rengaswemy. "Solid Oxide Fuel Cell Modeling." IEEE Transactions on Industrial Electronics 56, no. 1 (2009): 139-48.
- [8] Bianchi, Fiammetta Rita, Roberto Spotorno, Paolo Piccardo, and Barbara Bosio. "Solid Oxide Fuel Cell Performance Analysis through Local Modelling." Catalysts 10, no. 5 (2020): 519.
- [9] S. N. Ranasinghe and P. H. Middleton, "Modelling of single cell solid oxide fuel cells using COMSOL multiphysics," 2017 IEEE International Conference on Environment and Electrical Engineering and 2017 IEEE Industrial and Commercial Power Systems Europe (EEEIC / I&CPS Europe), Milan, Italy, 2017, pp. 1-6, doi: 10.1109/EEEIC.2017.7977790.
- [10] "How to navigate the COMSOL MULTIPHYSICS® user interface," COMSOL, https://www.comsol.com/support/learningcenter/article/How-to-Navigate-the-comsolmph-User-Interface-33881/12 (accessed Jun. 19, 2023).
- [11] F. Tietz, F. J. Dias, D. Simwonis, and D. Stöver, "Evaluation of commercial nickel oxide powders for components in solid oxide fuel cells," Journal of the European Ceramic Society, vol. 20, no. 8, pp. 1023-1034, 2000. doi:10.1016/s0955-2219(99)00271-x.
- [12] Y. Dong, L. Qi, I.-W. Chen, and J. Li, "A computational study of yttria-stabilized zirconia: II. Cation diffusion," in Acta Materialia, vol. 225, Oxford: Elsevier Science, pp. 438-450
- [13] S. P. Jiang, "Development of lanthanum strontium cobalt ferrite perovskite electrodes of solid oxide fuel cells a review," International Journal of Hydrogen Energy, vol. 44, no. 14, pp. 7448–7493, 2019. doi:10.1016/j.ijhydene.2019.01.212
- [14] R. P. O' Hayre, "Fuel cells for electrochemical energy conversion," NASA/ADS, Accessed October 2020. https://ui.adsabs.harvard.edu/abs/2017EPJWC.14800013O/abstract.
- [15] On the Maxwell-Stefan approach to multicomponent diffusion https://www.researchgate.net/publication/45928593_On_the_Maxwell-Stefan_Approach_to_Multicomponent_Diffusion
- [16] Lindstrom, Michael, and Brian Wetton. "A Comparison of Fick and Maxwell-Stefan Diffusion Formulations in PEMFC Gas Diffusion Layers." Heat and Mass Transfer 53, no.1 (2016): 205-12. doi:10.1007/s00231-016-1812-7.

- [17] "Multiphysics Cyclopedia." COMSOL. Accessed October, 2020. https://www.comsol.no/multiphysics
- [18] H. C. Brinkman, "A calculation of the viscous force exerted by a flowing fluid on a dense swarm of particles," Flow, Turbulence and Combustion, vol. 1, no. 1, p. 27, 1949.
- [19] M. Kobera, "Brinkman equations as a model for flows in porous media," in WDS'08 Proceedings of Contributed Papers, Part III, 2008, pp. 38–43.
- [20] D. Noren and M. Hoffman, "Clarifying the butlervolmer equation and related approximations for calculating activation losses in solid oxide fuel cell models," Journal of Power Sources, vol. 152, pp. 175 – 181, 2005.
- [21] K. S. T. Hosoia, T. Yonekuraa and K. Sasaki, "Exchange current density of SOFC electrodes: Theoretical relations and partial pressure dependencies rate-determined by electrochemical reactions," Journal of Electrochemical Society, vol. 162, pp. 136 – 152, 2015.
- [22] V. Ramani, "Fuel cells," The Electrochemical Society Interface, vol. 15, no. 1, pp. 41–44, 2006. doi:10.1149/2.f12061if.
- [23] Brajter-Toth, Anna. "Electrochemistry for Chemists, By Donald Sawyer (Texas A&M University), Andrzej Sobkowiak (Rzeszow University of Technology), and Julian L. Roberts, Jr. (University of Redlands). Wiley: New York. 1995. xv+ 505 pp. \$64.95. ISBN 0-471-59468-7." (1996): 10339-10340.
- [24] Barbir, F. (2013) 'Chapter Three Fuel Cell Electrochemistry', in PEM fuel cells: Theory and practice. Second. Amsterdam: Elsevier/Academic Press, pp. 33–72
- [25] Y. Lin and S. B. Beale, "Performance predictions in solid oxide fuel cells," Applied Mathematical Modelling, vol. 30, no. 11, pp. 1485-1496, 2006. doi:10.1016/j.apm.2006.03.009
- [26] Polarization curves Fuel Cell Store. Accessed October, 2020. Available at: https://www.fuelcellstore.com/blogsection/polarization-curves
- [27] L. Blanco-Cocom, S. Botello-Rionda, L. C. Ordóñez, and S. Ivvan Valdez, "A Self-Validating Method via the Unification of Multiple Models for Consistent Parameter Identification in PEM Fuel Cells," vol. 15, no. 3, pp. 885–885, Jan. 2022, doi: https://doi.org/10.3390/en15030885.
- [28] Testing the voltage and the power as a function of the current density. Accessed October 2020. https://joint-researchcentre.ec.europa.eu/document/download/e306c6c4-6f75-4114-82df 02b7fe55b25a_en?filename=Test%20Module%20PEFC%20SC%205-7.